JOURNAL OF SPACECRAFT AND ROCKETS
Vol. 42, No. 4, July–August 2005

Control of Hypersonic Turbulent Skin Friction by Boundary-Layer Combustion of Hydrogen

R. J. Stalker*
University of Queensland, Brisbane, Queensland 4072, Australia

Shvab–Zeldovich coupling of flow variables has been used to extend Van Driest's theory of turbulent boundary-layer skin friction to include injection and combustion of hydrogen in the boundary layer. The resulting theory is used to make predictions of skin friction and heat transfer that are found to be consistent with experimental and numerical results. Using the theory to extrapolate to larger downstream distances at the same experimental conditions, it is found that the reduction in skin-friction drag with hydrogen mixing and combustion is three times that with mixing alone. In application to flow on a flat plate at mainstream velocities of 2, 4, and 6 km/s, and Reynolds numbers from 3×10^6 to 1×10^8, injection and combustion of hydrogen yielded values of skin-friction drag that were less than one-half of the no-injection skin-friction drag, together with a net reduction in heat transfer when the combustion heat release in air was less than the stagnation enthalpy. The mass efficiency of hydrogen injection, as measured by effective specific impulse values, was approximately 2000 s.

Nomenclature

A	=	KU/υ^*
C_{pa}	=	constant pressure specific heat of air, (J/kg)K
C_{pi}	=	constant pressure specific heat of species i, (J/kg)K
C_{ps}	=	mixture specific heat, $= \sum_i c_i C_{pi}$, (J/kg)K
c_f	=	skin-friction coefficient, $2\tau/(\rho_e U^2)$
c_h	=	Stanton number, $\dot{q}_w/\{\rho_e U(H_e - C_{pa}T_w)\}$
c_i	=	mass fraction of species i
F_n	=	no-injection skin-friction drag
F_r	=	reduction in skin friction with injection
f	=	relative stoichiometric mass fraction of hydrogen, =0.125
$f c_{oe} \Delta Q$	=	heat released by combustion of hydrogen in air, =3.45 MJ kg^{-1}
g	=	u/U at flame front
$\bar{g}$	=	gravitational acceleration, m/s^2
H	=	stagnation enthalpy, $C_{ps}T + u^2/2$, MJ kg^{-1}
h	=	static enthalpy, MJ kg^{-1}
h_{io}	=	enthalpy of formation of species i
I	=	$C_{ps}T + \sum_i c_i h_{io} + \frac{u^2}{2}$
K	=	von Kármán constant, 0.41
k	=	molecular thermal conductivity, W · m · K
$\dot{m}$	=	mass flow of hydrogen added to the boundary layer, kg s^{-1} m^{-1}
P_r	=	Prandtl number, $(\mu C_{ps}/k)_w$
$\dot{Q}$	=	total heat transfer, W
$\dot{Q}_n$	=	total heat transfer with no injection, W
$\dot{q}$	=	heat transfer to wall, W/m^2
R	=	mixture dependent gas constant
R_{ex}	=	Reynolds number, $\rho_e U x/\mu_e$
T	=	temperature, K
T_{aw}	=	$T_e(1 + 0.5U^2/h_e)$
U	=	mainstream velocity, km/s
u	=	velocity in x direction
u_j	=	hydrogen injection velocity, km/s
x	=	distance along surface, m
y	=	distance normal to surface
Z	=	Shvab–Zeldovich coupling parameter
z	=	u/U
ΔQ	=	heat of combustion of hydrogen, 120 MJ kg^{-2}
δ	=	boundary-layer thickness
ε	=	combined molecular and eddy viscosities
θ	=	momentum thickness
μ	=	molecular viscosity
ν_w	=	kinematic viscosity, μ_w/ρ_w
ρ	=	density
τ	=	shear stress
υ	=	velocity in y direction
υ^*	=	friction velocity, $\sqrt{(\tau_w/\rho_w)}$
$\dot{\omega}_i$	=	time rate of change of species (i)

Subscripts

aw	=	adiabatic wall
e	=	mainstream
H	=	hydrogen
l	=	water
n	=	no hydrogen injection
o	=	oxygen
w, W	=	surface

Received 3 March 2004; revision received 6 July 2004; accepted for publication 6 August 2004.

*Emeritus Professor, Mechanical Engineering, School of Engineering, Faculty of Engineering, Physical Sciences and Architecture. Fellow AIAA.

Introduction

THE development of slender hypervelocity vehicles can offer the possibility of economical transportation to and from low Earth orbit. The size and operating altitudes of these vehicles are likely to be such that predominantly turbulent boundary layers can be expected on their flow surfaces, leading to substantial reductions in their performance caused by skin friction drag.

An example of this performance reduction is seen in Fig. 39 of Ref. 1, where it is shown that, in calculating the performance of a single-stage-to-orbit vehicle, the drag was increased by 13% and the payload halved if fully turbulent boundary layers were assumed rather than laminar ones.

Figure 1 displays a further example, by showing the effect of turbulent skin friction on the lift-to-drag ratio of a 20-m-long waverider caret delta wing with the windward surface at an incidence of 5 deg and the upper surface at zero incidence. The wing dihedral is varied to maintain on-design flow as the Mach number changes, and the trailing-edge Reynolds number on the windward surface is

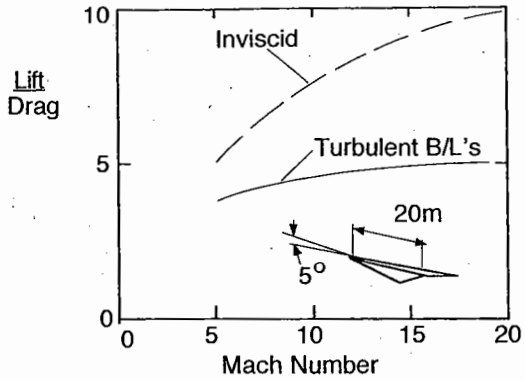

Fig. 1. Aerodynamic performance and skin-friction drag.

maintained at 10^8. Large reductions in the lift-to-drag ratio are caused by turbulent skin friction, an effect that would be manifested, for example, in a reduced reentry footprint for such vehicles.

Clearly, turbulent skin friction has an important effect on vehicle performance, and it is worthwhile considering means of controlling turbulent skin-friction levels. One such means is the injection and combustion of hydrogen in the boundary layer. Shock-tunnel experiments[2] have indicated that large reductions in skin friction can be obtained by this method. The purpose of this paper is to report an analysis that is consistent with these results and allows ready prediction of potential skin-friction reduction at other conditions.

A number of analyses exist[3–7] of skin friction in compressible turbulent boundary layers. All of these analyses are semi-empirical in nature and involve somewhat arbitrary assumptions. The analysis by Van Driest[3,4] has proven popular among experimentalists, particularly in the form of Van Driest II,[4] and the assumptions on which it is based can readily be extended to take account of combustion in the boundary layer. Therefore it will be used as the basis of the present analysis.

The effect of turbulent boundary-layer combustion on skin friction has received attention in the past at low subsonic air speeds. Kulgein[8] found that, with boundary-layer combustion of methane injected through a porous wall, no reaction-induced effect on skin friction was observed. Porous wall experiments, with hydrogen fuel diluted by nitrogen, were also done by Wooldridge and Muzzy.[9] Relatively low hydrogen mass fractions were used in these experiments, but they yielded the encouraging result that measured boundary-layer profiles indicated turbulent Prandtl and Schmidt numbers (and hence, Lewis number), which could be taken as unity. This is a commonly used assumption in turbulent boundary-layer analysis and is employed in the following analysis. Jones et al.[10] conducted a similar study, with particular attention to velocity profiles, and pointed to a large reduction in skin friction obtained with combustion in constant pressure flows. A recent numerical study[11] showed that heating within a turbulent boundary layer at a Mach number of three could produce large skin-friction reductions, but the study did not consider a combustion model. Thus, although there is a history of research on combustion in turbulent boundary layers, a quantitative appreciation of the effect of hydrogen combustion in supersonic and hypersonic turbulent boundary layers is not yet available. There exists a substantial literature on foreign gas injection into turbulent boundary layers, involving both injection through a porous surface and slot injection. The latter is of particular interest here, and a useful introduction to the subject is given by Hefner and Bushnell.[12]

After a brief review of Van Driest's theory, the paper discusses the combustion model and then proceeds to develop an analysis that yields formulas for skin friction, heat transfer, and mass flow of injected hydrogen with and without combustion. The features of the hydrogen-injected boundary-layer flow at a representative mainstream stagnation enthalpy are then explored, before the predicted results are compared with the results of previous experiments and numerical analysis. Finally, the analysis is used to predict the effect of injected-hydrogen mass flow on the skin-friction drag and net heat transfer on a flat plate at a range of mainstream velocities before concluding.

Van Driest

As the mainstream Mach number is increased, boundary-layer temperatures also increase. This causes different effects in laminar and turbulent boundary layers. In the laminar boundary layer the resulting reduction in density tends to increase the width, normal to the surface, of the boundary-layer streamtubes, tending to reduce the shear stress. However, this tendency is partially offset by the temperature-induced increase in viscosity, leading only to modest reductions in skin friction. In the turbulent case the shear stress is mainly caused by the Reynolds stresses, which are directly dependent on density, and therefore the turbulent viscosity tends to be reduced, rather than increased, by increases in temperature, leading to larger reductions in skin friction than in the laminar case.

Van Driest's analysis[3] seeks to adequately represent the effect on skin friction of temperature-induced density changes in the turbulent boundary layer. It applies to constant pressure flow of a perfect gas with a uniform surface temperature. Because the pressure is constant across the boundary layer, the density is inversely proportional to the temperature, which, assuming $P_r = 1$, can be obtained from the linear variation of stagnation enthalpy with velocity expressed in the Crocco relation. This results in the relation

$$\rho_w/\rho = 1 + bz - a^2 z^2 \tag{1}$$

where $a^2 = U^2/2H_w$ and $b = (H_e - H_w)/H_w$.

For Van Driest II,[4] the shear stress is given by Prandtls mixing length equation, with the von Kármán mixing length, that is,

$$\tau = \rho K^2 \left(\frac{\mathrm{d}u}{\mathrm{d}y}\right)^4 \Big/ \left(\frac{\mathrm{d}^2 u}{\mathrm{d}y^2}\right)^2 \tag{2}$$

It is then assumed that the shear stress τ is constant at its surface value τ_w, and using Eq. (1), Eq. (2) is integrated to yield a relation for $\mathrm{d}y/\mathrm{d}u$. This relation and Eq. (1) are used, together with the definition of θ, that is,

$$\theta = \int_o^{z=1} \left(\frac{\rho}{\rho_e}\right)(1-z)z\,\mathrm{d}y \tag{3}$$

to obtain an integral expression for θ. This is integrated into a series form through successive integration by parts. Then, taking the leading terms of the series, employing the further relation

$$c_f = \frac{2\,\mathrm{d}\theta}{\mathrm{d}x} \tag{4}$$

and noting that $c_f \ll 1$, an expression for c_f is obtained. Constants in the expression are adjusted to match the incompressible Kármán–Schoenherr skin-friction formula, yielding

$$4.15\log_{10}(R_{ex}c_f\mu_e/\mu_s) + 1.7 = F_o[c_f(T_{aw} - T_e)/T_e]^{-\frac{1}{2}} \tag{5}$$

where

$$F_o = \sin^{-1}[(2a^2 - b)/Q] + \sin^{-1}(b/Q), \qquad Q = (b^2 + 4a^2)^{\frac{1}{2}}$$

Van Driest's theory has been successful in predicting skin friction with widely varying boundary-layer density distributions. Thus, it predicts the variation of skin friction in passing from low supersonic to hypersonic flows on adiabatic flat plates,[13] on cooled flat plates,[14] and on room-temperature flat plates in shock tunnels at Mach numbers up to 13 with stagnation enthalpies up to 2 MJ/kg (Ref. 15), and at Mach numbers near 6 with stagnation enthalpies up to 13 MJ/kg (Ref. 16). By use of the Reynolds analogy, it also predicts the heat transfer to a 5-deg half-angle cone in free flight at a Mach number of 20 (Ref. 17). In view of this success, it seems not unreasonable to expect that the effect on skin friction of boundary-layer density changes associated with hydrogen injection and combustion might also be amenable to an analysis which follows that leading to Eq. (5).

Flow Model

It is assumed that the combustion reaction between hydrogen and oxygen can be represented as

$$2H_2 + O_2 \rightarrow 2H_2O + 2\Delta Q \tag{6}$$

so that there is no dissociation of water formed, and the reaction occurs spontaneously when the two reactant gases come in contact, regardless of the temperature. Thus, hydrogen and oxygen in the molecular form cannot coexist at any point within the boundary layer. It is well known that the reaction is much more complicated in reality and that the time taken for the reaction to proceed to completion increases so dramatically with reductions in temperature that approximately 800 K can be taken as an ignition temperature. However, except at very low hypersonic Mach numbers, temperatures exceeding 800 K can be expected to occur over a substantial part of a hypersonic boundary layer, and, once combustion begins somewhere in the boundary layer, conduction of the heat released will raise the temperature in other parts of the boundary layer. Thus, although the model might tend to somewhat overestimate the heat release within the boundary layer, and therefore overestimate the effects of combustion, it can be expected to provide an upper limit and a first approximation for those effects. Moreover, it is recommended by its simplicity.

Boundary-layer flow with hydrogen injection and combination is represented in Fig. 2. The two-dimensional boundary layer is formed on a flat plate in the absence of pressure gradients. As shown in Fig. 2a, hydrogen is injected, parallel to the surface, from a slot, and the boundary layer passes through a number of regions in its downstream development. In region (i), a process of flow adjustment takes place to yield a constant pressure across the boundary layer. In region (ii), a layer of hydrogen exists close to the surface and is separated from the mainstream by a layer where hydrogen and air mix. Thus, for regions (i) and (ii), $c_{HW} = 1$. If sufficient hydrogen is injected, this region can extend over a large downstream distance. However, the present analysis does not consider this case and is therefore restricted to hydrogen mass flows such that region (ii) does not exist or is of very short extent. Therefore it might be neglected for a flow model. In region (iii) $1 \geq c_{HW} \geq 0$, and the boundary layer enters a process of long-term growth, with the local hydrogen mass fraction reducing with downstream distance as the hydrogen present is mixed with the additional air entrained in the boundary layer and as hydrogen is converted to water by combustion. In region (iv), where $c_{HW} = 0$, all of the hydrogen is burned, and it is present only as water.

The flow in regions (iii) and (iv) of Fig. 2a is represented by the simplified model shown in Fig. 2b. It is assumed that region (iii) begins immediately at the leading edge. Thus hydrogen is present in the gas mixture at the surface and sets up a diffusion gradient through the boundary layer toward a flame front. Hydrogen is injected continuously along the surface, to compensate for the diffusion of hydrogen away from the surface, and maintains a constant value of the hydrogen surface mass fraction. This implies that the boundary conditions of Fig. 2a differ from those of Fig. 2b, but, as outlined next, the two can be related piecewise by using local similarity. At any station along the plate, no oxygen is present on the surface side of the flame front because it has all been removed by combustion at the flame front upstream of the station, and hydrogen diffuses from the surface to the flame front, where it undergoes combustion. On the mainstream side of the flame front, no hydrogen is present because all of the hydrogen reaching the flame front is consumed there, and oxygen diffuses from the mainstream to the flame front. In region (iv), the hydrogen concentration at the surface falls to zero, and the presence of water is associated with a nonzero concentration of oxygen. The flame front disappears, and water diffuses from the surface towards the mainstream.

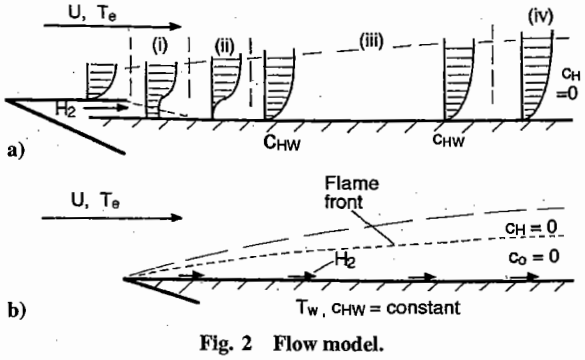

Fig. 2 Flow model.

The model of Fig. 2b, with species mass fractions constant along the surface, is used to obtain the boundary-layer profiles, which are then applied to the flow of Fig. 2a. As already noted, the species mass fractions of Fig. 2a are not constant along the surface, but, as will be seen next, the variation with downstream distance is sufficiently small that the local similarity approximation[18] can be applied. This approximation allows the local flow solutions to be obtained from the local flow properties, independent of the upstream variation of flow conditions. Thus, as the flow in regions (iii) and (iv) of Fig. 2a develops in the downstream direction, it passes through a series of flow solutions, each one corresponding to a solution of the flow of Fig. 2b. For each of these solutions, the boundary conditions are invariant along the surface, and the analysis of Van Driest can therefore be extended to include hydrogen injection and combustion, as described in the following analysis.

The analysis presented considers only region (iii), where the hydrogen mass fraction at the surface lies between unity and zero. In region (iv), where hydrogen is present only as water, the analysis shows that the expected skin-friction reduction is too small to be of interest here.

Analysis

Boundary-Layer Density

Combining the turbulent and the molecular transport coefficients, and taking the resultant Lewis numbers and Prandtl numbers as unity, the two-dimensional turbulent boundary-layer equations for momentum, species, and energy transfer with zero pressure gradient, can be written as[19]

$$\rho u \frac{\partial u}{\partial x} + \rho v \frac{\partial u}{\partial y} = \frac{\partial}{\partial y}\left(\varepsilon \frac{\partial u}{\partial y}\right) \tag{7}$$

$$\rho u \frac{\partial c_i}{\partial x} + \rho v \frac{\partial c_i}{\partial y} = \frac{\partial}{\partial y}\left(\varepsilon \frac{\partial c_i}{\partial y}\right) + \rho \dot{\omega}_i \tag{8}$$

$$\rho u \frac{\partial I}{\partial x} + \rho v \frac{\partial I}{\partial y} = \frac{\partial}{\partial y}\left(\varepsilon \frac{\partial I}{\partial y}\right) \tag{9}$$

It is assumed that the specific heat of each of the species remains constant as the temperature and mass fractions change, that is, C_{pi} remains constant as the temperature changes, to write

$$I = C_{ps}T + \sum_i c_i h_{io} + \frac{u^2}{2} \tag{10}$$

Noting that unit mass of oxygen reacts with f mass units of hydrogen to produce $(1+f)$ mass units of water, it follows that the time rate of change of the species is related by

$$\frac{\dot{\omega}_H}{f} = \dot{\omega}_o = \frac{-\dot{\omega}_l}{(1+f)} = -\rho \frac{\sum_i \dot{\omega}_i h_{io}}{f \Delta Q} \tag{11}$$

Multiplying each of Eqs. (8) by the appropriate h_{io}, summing the resultant equations, and subtracting from Eq. (9) yields

$$\rho u \frac{\partial H}{\partial x} + \rho v \frac{\partial H}{\partial y} = \frac{\partial}{\partial y}\left(\varepsilon \frac{\partial H}{\partial y}\right) - \rho \sum_i \dot{\omega}_i h_{io}$$

Then, with the Shvab–Zeldovich coupling[20] parameters $Z_{HO} = c_O - c_H/f$, $Z_{OT} = c_O + H/(f\Delta Q)$ and $Z_{HT} = c_H + H/\Delta Q$, using Eqs. (8), (10), and (11) allows an equation identical in form to Eq. (7) to be written for each of the coupled variables, leading to a relation

$$Z = d_1 + d_2 u \tag{12}$$

where $Z = Z_{HO}$, Z_{OT}, or Z_{HT}, and d_1 and d_2 are constants that are determined from the boundary conditions for each of the coupled variables. The boundary conditions at the wall are $u = 0$, $c_o = 0$, and $c_H = c_{HW}$, whereas in the mainstream they are $u = U$, $c_o = c_{oe}$, and $c_H = 0$, and $c_H = c_o = 0$ at the flame front where $u/U = g$. Evaluating Z_{HO} then leads to

$$g = c_{HW}/(c_{HW} + f c_{oe}) \tag{13}$$

Thus, the flame front moves closer to the wall as the mass fraction of hydrogen at the wall is reduced.

Applying the same procedures to evaluate Z_{OT} and Z_{HT}, expressions for H on both sides of the flame front are obtained, leading to,

for

$$0 < z < g, \qquad C_{ps}T/H_W = 1 + b_1 z - a^2 z^2 \tag{14}$$

and for

$$g < z < 1, \qquad C_{ps}T/H_W = 1 + \alpha + b_2 z - a^2 z^2 \tag{15}$$

where

$$H_W = C_{psw} T w, \qquad a^2 = U^2/(2H_W), \qquad \alpha = c_{HW}\Delta Q/H_W$$

$$b_1 = (H_e - H_W + f c_{oe}\Delta Q)/H_W$$

$$b_2 = (H_e - H_W - c_{HW}\Delta Q)/H_W$$

Now, because the pressure remains constant across the boundary layer

$$\rho_w/\rho = [(RC_{psw})/(R_w C_{ps})]C_{ps}T/H_W \tag{16}$$

Further, by using the Shvab–Zeldovich coupling $Z_{ol} = c_o + c_l/(1+f)$ (i.e., the total mass fraction of oxygen atoms), together with the wall boundary condition that the ratio of the mass fraction of oxygen atoms to the mass fraction of nitrogen atoms is equal to its mainstream value of 0.286, it can be shown that the ratio remains at that value throughout the boundary layer. Thus, with $C_{pH} = 14.07C_{pa}$, $C_{pl} = 1.985C_{pa}$, $C_{po} = 0.904C_{pa}$, and $C_{pN} = 1.028C_{pa}$, it is found that, for $0 \le z \le g$,

$$C_{ps} = 12.8(c_H + 0.098)C_{pa} \tag{17}$$

$$\frac{RC_{psw}}{R_w C_{ps}} = \frac{(c_H + 0.088)}{(c_H + 0.098)} \frac{(c_{HW} + 0.098)}{(c_{HW} + 0.088)} \tag{18}$$

while, for $g \le z \le 1$,

$$C_{ps} = (1 + 1.07c_l)C_{pa} \tag{19}$$

$$\frac{RC_{psw}}{R_w C_{ps}} = 0.968 \frac{(1 + 0.689c_l)}{(1 + 1.07c_l)} \frac{(c_{HW} + 0.098)}{(c_{HW} + 0.088)} \tag{20}$$

Plotting Eqs. (18) and (20) in Fig. 3a, it is clear that a good approximation to Eq. (16) is

$$\rho_w/\rho = C_{ps}T/H_W \tag{21}$$

and that this yields a maximum error of only 10% at $z = g$. Substitution of Eq. (21) in Eqs. (14) and (15) then provides the density as two quadratic relations in velocity. These relations are similar to Eq. (1), as used by Van Driest, with the coefficients changed to include to include the effects of combustion.

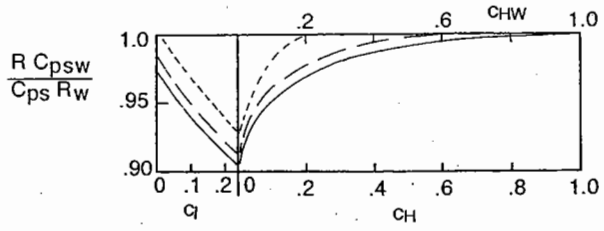

a) Density factor

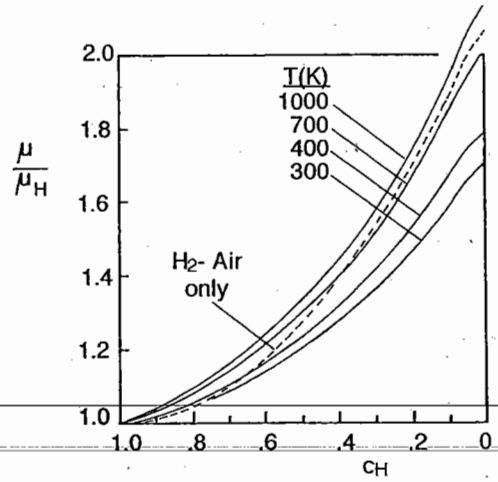

b) Molecular viscosity of H_2—Air and H_2—H_2O—N_2 mixture with $c_l = 0.32c_{N_2}$

Fig. 3 Gas mixture properties.

Momentum Thickness

The skin friction is to be obtained from a boundary-layer momentum balance involving the momentum thickness, and this requires knowledge of the boundary-layer velocity profile. Following Van Driest, this is obtained by integrating Eq. (2) with $\tau = \tau_W$ to yield

$$v^* \ell_n\left(\frac{dy}{du}\right) + \text{constant} = K \int \sqrt{\frac{\rho}{\rho_W}}\, du \tag{22}$$

For $0 \le z \le g$, Eqs. (21) and (14) are used to substitute for ρ/ρ_W on the right-hand side of Eq. (22), and the integration is performed from $z = 0$ to z, to obtain

$$\frac{dy}{dz} = U\left[\frac{\nu_W}{(v^*)^2}\right] \exp\left(B_o - \left(\frac{KU}{av^*}\right)\left\{\sin^{-1}\left[\frac{(b_1 - 2a^2 z)}{Q_1}\right] - \sin^{-1}\left(\frac{b_1}{Q_1}\right)\right\}\right) \tag{23}$$

where B_o is a constant and $Q_1 = \sqrt{(b_1^2 + 4a^2)}$.

Similarly, for $g \le z \le 1$, by using Eqs. (21) and (15),

$$\frac{dy}{dz} = U\left[\frac{\nu_W}{(v^*)^2}\right] \exp\left(B_1 + \left(\frac{KU}{av^*}\right)\left\{\sin^{-1}\left[\frac{(b_2 - 2a^2)}{Q_2}\right] - \sin^{-1}\left[\frac{(b_2 - 2a^2 z)}{Q_2}\right]\right\}\right) \tag{24}$$

where $Q_2 = \sqrt{[b_2^2 + 4a^2(1+\alpha)]}$ and B_1 is a constant, which can be related to B_o by equating the two relations for dy/dz at $z = g$.

Equation (3) for the momentum thickness is written in the form

$$\theta = \left(\frac{\rho_W}{\rho}\right)\left[\int_o^g \left(\frac{\rho}{\rho_W}\right)(1-z)z\,\mathrm{d}y + \int_g^1 \left(\frac{\rho}{\rho_W}\right)(1-z)z\,\mathrm{d}y\right] \tag{25}$$

Following Van Driest, the first integral on the right-hand side of Eq. (25) can be developed into a series in A^{-1} by noting that

$$\left(\frac{\mathrm{d}}{\mathrm{d}z}\right)\left(\exp\left\{\left(\frac{A}{a}\right)\sin^{-1}\left[\frac{(2a^2z-b_1)}{Q_1}\right]\right\}\right)$$

$$= \left(\frac{A}{\sqrt{1+b_1z-a^2z^2}}\right)\exp\left\{\left(\frac{A}{a}\right)\sin^{-1}\left[\frac{(2a^2z-b_1)}{Q_1}\right]\right\}$$

and employing this relation in successive integration by parts. Because $A \gg 1$, only terms in A^{-1} and A^{-2} are retained. A similar process can be carried out for the second integral on the right-hand side of Eq. (25), but the terms in the resultant series are oscillatory divergent for $z \to 1$ when $h_e \ll H_W$, $\alpha \gg 1$, and $|b_2| \gg 1$. The use of hydrogen with $c_{HW} = \mathcal{O}(1)$ ensures that these conditions will normally be met. Fortunately, by using the approximation $(1-z) \ll 1$, it can be shown that when the terms in A^{-1} and A^{-2} are subtracted from the integral the remainder is of order A^{-3}, and therefore it is again only necessary to retain the terms in A^{-1} and A^{-2} for a satisfactory approximation to the integral. Thus, by adding the resultant expressions for the two integrals of Eq. (25), it is found that

$$\theta = UA^{-2}\left\{\rho_W v_W \Big/ \left[\rho_e (v^*)^2\right]\right\}\exp[B_o + (A/a)F_1]$$
$$\times \{1 + G\exp[(A/a)(F_2 - F_1)]\} \tag{26}$$

where

$$G = 0.5(b_1 - b_2)g(1-g)\Big/\left(1 + b_1 g - a^2 g^2\right) \tag{27}$$

$$F_1 = \sin^{-1}(b_1/Q_1) + \sin^{-1}\left[\left(2a^2 - b_2\right)\Big/Q_2\right]$$
$$+ \sin^{-1}\left[\left(2a^2 g - b_1\right)\Big/Q_1\right] - \sin^{-1}\left[\left(2a^2 g - b_2\right)\Big/Q_2\right] \tag{28}$$

$$F_2 = \sin^{-1}(b_1/Q_1) + \sin^{-1}\left[\left(2a^2 g - b_1\right)\Big/Q_1\right] \tag{29}$$

Hydrogen Mass Flow

The total mass flow of hydrogen in the boundary layer can be related to θ by noting that the local mass fraction of hydrogen, both burned and unburnt, is given by the Shvab–Zeldovich coupling $Z_{HI} = c_H + c_I f/(1+f)$. By employing Eq. (12), the boundary conditions $Z_{HI} = 0$ when $z = 1$, and $Z_{HI} = c_{HW} + c_{IW} f/(1+f)$ when $z = 0$, can be used to obtain

$$Z_{HI} = \{c_{HW} + c_{IW} f/(1+f)\}(1-z)$$

and, because the ratio of total mass fraction of oxygen atoms at the surface to the mass fraction of nitrogen atoms is the same as in the mainstream, this becomes

$$Z_{HI} = (c_{HW} + f c_{oe})(1-z)/(1+f c_{oe})$$

Now, the total mass flow of hydrogen in the boundary layer is given by

$$\dot{m} = \int_o^\delta Z_{HI}\rho u\,\mathrm{d}y$$

which

$$= \left\{\frac{(c_{HW} + f c_{oe})}{(1+f c_{oe})}\right\}\rho_e U\int_o^{z=1}\left(\frac{\rho}{\rho_e}\right)(1-z)z\,\mathrm{d}y$$

and therefore, recalling Eq. (3),

$$\dot{m} = \{(c_{HW} + f c_{oe})/(1+f c_{oe})\}\rho_e U\theta \tag{30}$$

Thus, to maintain the uniform boundary conditions of Fig. 2b, the total hydrogen mass flow must increase with the boundary-layer momentum thickness.

Skin-Friction and Hydrogen Mass Flow

Remembering that, at this stage, the analysis assumes continuous hydrogen injection along the surface, a relation for the skin friction c_f can now be obtained by taking the momentum balance for the boundary layer and differentiating with respect to x, to yield

$$\tau_W + (U - u_j)\frac{\mathrm{d}\dot{m}}{\mathrm{d}x} = \frac{\rho_e U^2\,\mathrm{d}\theta}{\mathrm{d}x}$$

which becomes, on employing Eq. (30),

$$c_f = 2\left(\frac{\mathrm{d}\theta}{\mathrm{d}x}\right)\frac{[1 - c_{HW} + (c_{HW} + f c_{oe})u_j/U]}{(1+f c_{oe})} \tag{31}$$

Substituting for θ from Eq. (26), collecting all terms involving A and integrating while noting that as $x \to 0$, $c_f \to \infty$, and $A \to 0$, then remembering that $A \gg 1$ for $c_f \ll 1$, an implicit relation for c_f can be obtained as

$$c_f R_{ex}\mu_e/\mu_W = 2\left(K^{-2}\exp B_o\right)(1+f c_{oe})^{-1}[1 - c_{HW}$$
$$+ (c_{HW} + f c_{oe})u_j/U]\exp\left(Ka^{-1}\sqrt{2/c_f}\sqrt{\rho_W/\rho_e}F_1\right)$$
$$\times\left\{1 + G\exp\left[Ka^{-1}\sqrt{2/c_f}\sqrt{\rho_W/\rho_e}(F_2 - F_1)\right]\right\},$$

This equation must reduce to Eq. (5) when the hydrogen mass flow, given by Eq. (30), is zero, and therefore the constants in the equation are adjusted to satisfy this requirement. Thus, with $B_o = -3.46$, the resulting relation is

$$4.15\log(c_f R_{ex}\mu_e/\mu_w) + 1.7$$
$$= F_1\Big/\sqrt{c_f(T_{aw} - T_e)/T_e} + 3.97\log\{[1 - c_{HW} + (c_{HW}$$
$$+ f c_{oe})u_j/U]/(1+f c_{oe})\} + 3.97\log\left\{1 + G\right.$$
$$\left.\times\exp\left[(F_2 - F_1)K\sqrt{2}\Big/\sqrt{c_f(T_{aw} - T_e)}\Big/T_e\right]\right\} \tag{32}$$

where the coefficient of the first term on the left-hand side has been raised from 3.97 to 4.15. In this term the molecular viscosity of air μ_e is given by the Sutherland formula as $\mu_e = [6.59\times10^{-3}/(111+T)](T/273)^{1.5}$, whereas that for hydrogen is 49% of the value for air and, to within 3%, follows the same variation with temperature up to 1000 K (Ref. 21). Because all of the oxygen is burned on the wall side of the flame front, a hydrogen-steam-nitrogen mixture is present at the wall, with the mole fraction of steam one-half that of nitrogen. The viscosity for the mixture is calculated using Wilke's method,[22] and the effect of hydrogen mixture ratio is presented in Fig. 3b for temperatures ranging from 300 to 1000 K. The increase in viscosity with temperature is caused by the relatively greater sensitivity to temperature of the viscosity of steam.

The total mass flow of hydrogen is obtained by substituting from Eq. (26) into Eq. (30), and putting $B_o = -3.46$, to yield

$$\dot{m} = 0.187\mu_W[(c_{HW} + f c_{oe})/(1+f c_{oe})]$$
$$\times\exp\left[F_1 K\sqrt{2}\Big/\sqrt{c_f(T_{aw} - T_e)/T_e}\right]$$
$$\times\left\{1 + G\exp\left[(F_2 - F_1)K\sqrt{2}\Big/\sqrt{c_f(T_{aw} - T_e)/T_e}\right]\right\} \tag{33}$$

Thus, Eqs. (32) and (33) allow the skin friction, and the associated mass flow injected into the boundary layer, to be determined.

Heat Transfer

No reactions take place at the surface, so that the heat transfer is caused by conduction alone, which depends on the temperature gradient at the surface. This can be obtained by writing Eq. (14) in the form

$$C_{ps}T = H_W + (H_e - H_W + fc_{oe}\Delta Q)u/U - u^2/2$$

differentiating with respect to y, and putting $u = 0$, to obtain

$$C_{psw}\frac{dT}{dy} = (H_e - H_W + fc_{oe}\Delta Q)\left(\frac{du}{dy}\right)\Big/U - T_W\left(\frac{dC_{ps}}{dy}\right) \tag{34}$$

at the surface. The specific heat C_{ps} is given by Eq. (17) and involves c_H, which can be obtained from the Shvab–Zeldovich coupling parameter $Z_{HO} = c_o - c_H/f$. Noting that $c_o = 0$ for $0 \le z \le g$, and taking boundary conditions at $z = g$, where $c_o = c_H = 0$, and at the wall, it is found that $c_H = c_{HW} - (c_{HW} + fc_{oe})z$. Thus, by employing Eq. (17),

$$\left(\frac{dC_{ps}}{dy}\right) = -12.8C_{pa}(c_{HW} + fc_{oe})\left(\frac{du}{dy}\right)\Big/U$$

and noting that $\dot{q}_W = k_W(dT/dy)$, while $\tau_W = \mu_W(du/dy)$, Eq. (34) yields

$$\dot{q}_W = \tau/(UP_r)[H_e + fc_{oe}\Delta Q - 12.8C_{pa}T_W(0.098 - fc_{oe})]$$

because $f = 0.125$ and $c_{oe} = 0.22$ for hydrogen air, the Stanton number can be written

$$c_h = c_f/(2P_r)(H_e + fc_{oe}\Delta Q - 0.90C_{pa}T_W)/(H_e - C_{pa}T_W) \tag{35}$$

This is an approximation because of the approximation for C_{ps} in Eq. (17). Without this approximation the Stanton number without hydrogen injection is

$$c_{hn} = 0.5c_{fn}/P_{rn} \tag{36}$$

This equation gives the Reynolds analogy factor $2c_{hn}/c_{fn}$ as P_{rn}, which is because of the use of the Crocco relation for the variation of T with u. Differing experiments with hypersonic turbulent boundary layers under cold wall conditions[16] indicate that, rather than taking $P_{rn} = 0.72$, as obtained from the molecular coefficients, it is a better approximation to take $P_{rn} = 1$. In the present case, calculations, based on molecular properties,[21,22] indicate that P_r for the hydrogen-water-nitrogen mixture formed at the surface varies by only ±17% as the hydrogen mass fraction changes from zero to one. It is therefore reasonable to assume that P_r will behave as P_{rn}, and that $P_r = 1$. The ratio of the two Stanton numbers of Eqs. (35) and (36) then can be written

$$c_h/c_{hn} = (c_f/c_{fn})(H_e + fc_{oe}\Delta Q - 0.90C_{pa}T_W)/(H_e - C_{pa}T_W) \tag{37}$$

A correlation of experimental results for the Reynolds analogy factor, presented as Fig. 16 of Ref. 16, indicates that it varies with the skin-friction level. It is not known if this correlation would apply for the substantial reductions of skin friction that occur in the present case, and it is not taken into account. Thus some uncertainty surrounds the application of Eq. (37), implying a particular need for comparison with experiment.

Hydrogen Injection Without Combustion

If no combustion takes place, there is no flame front, $\Delta Q = 0$, $b_1 = b_2 = b$, $Q_1 = Q_2 = Q$, $F_1 = F_2 = F_0$, and Eqs. (14) and (15) reduce to Eq. (1). No water is formed, and Eq. (17) for the specific heat of the hydrogen-air mixture becomes

$$C_{ps} = 13.2(c_H + 0.076)C_{pa} \tag{38}$$

whereas Eq. (21) remains a good approximation for ρ_w/ρ. Noting that

$$c_H = c_{HW}(1 - z) \tag{39}$$

Eq. (30) for the mass flow of hydrogen in the boundary layer is replaced by

$$\dot{m} = c_{HW}\rho_e U\theta \tag{40}$$

and therefore the relation for the skin-friction coefficient corresponding to Eq. (4) is

$$c_f = 2\left(1 - c_{HW} + \frac{c_{HW}u_j}{U}\right)\frac{d\theta}{dx}$$

Thus, following the procedure that led to Eq. (5) yields the skin-friction relation

$$4.15\log(R_{ex}c_f\mu_e/\mu_w) = F_o\Big/\sqrt{c_f(T_{aw} - T_e)/T_e} + 3.97\log(1 - c_{HW} + c_{HW}u_j/U) \tag{41}$$

with F_o as defined for Eq. (5). The variation of the molecular viscosity at the wall μ_w with hydrogen mass fraction is presented in Fig. 3b for a hydrogen–air mixture.

The hydrogen mass flow is obtained from Eq. (33) by noting that, because $b_1 = b_2$ in Eq. (27), $G = 0$ and with Eq. (40) replacing Eq. (30), Eq. (33) becomes

$$\dot{m} = 0.187\mu_W c_{HW}\exp\left[F_oK\sqrt{2}\Big/\sqrt{c_f(T_{aw} - T_e)/T_e}\right] \tag{42}$$

The heat-transfer rate is obtained by putting $\Delta Q = 0$ in Eq. (34), which then becomes

$$C_{ps}\left(\frac{dT}{dy}\right) = (H_e - H_W)\left(\frac{du}{dy}\right)\Big/U - T_W\left(\frac{dC_{ps}}{dy}\right)$$

Using Eq. (38) for C_{ps}, together with Eq. (39), then leads to

$$\dot{q}_w = [\tau/(UP_r)](H_e - 1.00C_{pa}T_w)$$

and so the Stanton number can be written as

$$c_h = 0.5c_f/P_r$$

Again following the experimental evidence, which favors a Reynolds analogy factor of unity, it is assumed that $P_r = 1$ and therefore that

$$c_h = 0.5c_f \tag{43}$$

Analytic Results and Discussion

To fix ideas, it is convenient at this point to limit the discussion to consideration of a mainstream stagnation enthalpy of 7.54 MJ/kg, corresponding to a flight Mach number of 12.7. Not only does this stagnation enthalpy correspond to the experimental results discussed next, but it is also in the midrange of the flight velocities of interest (i.e., 2–6 km/s) and therefore can be expected to exhibit boundary-layer behavior that is typical over the range of stagnation enthalpies.

Local Similarity and the Effect of Combustion

Figure 4 displays the skin friction, obtained by using Eq. (32), and the corresponding total mass flow of hydrogen, burnt and unburnt, given by Eq. (33), for a range of Reynolds numbers. A mainstream temperature of 1500 K, a surface temperature of 300 K, a mainstream velocity of 3.38 km/s, and a hydrogen injection velocity of 1.55 km/s was used for the figure, and the effect of varying these is discussed next.

Each value of c_{HW}, the hydrogen surface mass fraction, represents a different flow model of the type shown in Fig. 2b, and for each flow model the total mass flow of hydrogen in the boundary layer increases with the Reynolds number. Maintaining a constant hydrogen mass flow as the Reynolds number increases, as in Fig. 2a,

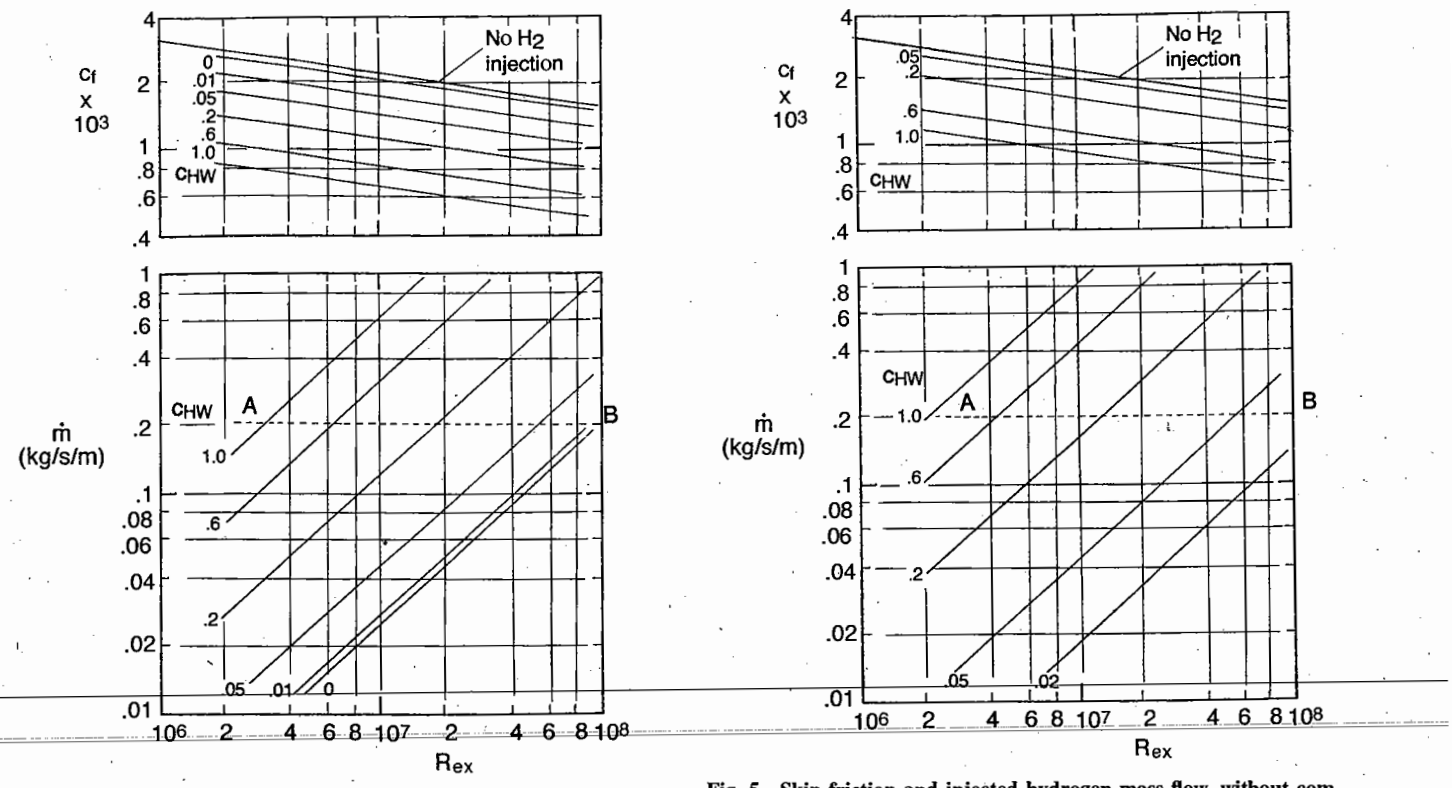

Fig. 4 Skin friction and injected hydrogen mass flow, with combustion: $H_e = 7.54$ MJ/kg, $T_e = 1500$ K, $T_w = 300$ K, $U_e = 3.38$ km/s, and $u_j = 1.55$ km/s.

Fig. 5 Skin friction and injected hydrogen mass flow, without combustion: $H_e = 7.54$ MJ/kg, $T_e = 1500$ K, $T_w = 300$ K, $U_e = 3.38$ km/s, and $u_j = 1.55$ km/s.

implies passing through a sequence of flow models, but, if local similarity applies, the boundary layer in the flow model corresponding to a given surface hydrogen mass fraction and Reynolds number will be identical to the constant hydrogen mass flow boundary layer at that surface hydrogen mass fraction and Reynolds number. Now, inspection of Fig. 4 indicates that a 10% change in skin friction is accomplished as R_{ex} increases by approximately 50% at constant hydrogen mass flow. Because the boundary-layer thickness is of the order of $x/R_{ex}^{0.2}$, this 50% increase in R_{ex} corresponds to the order of 10 boundary-layer thicknesses at the Reynolds numbers of interest. This is sufficient (e.g., Ref. 23) to allow the boundary layer to adjust to the change in boundary conditions implied by a 10% change in skin friction, thus allowing use of the local similarity approximation. Therefore the effect of hydrogen injection depends only on the total amount injected, and not on the distribution of injection along the surface.

Figure 4 shows that very substantial reductions in skin-friction coefficient are associated with mixing and combustion of hydrogen in the boundary layer. Because of the low density of hydrogen, boundary-layer densities tend to be reduced by mixing without combustion, and, as shown in Fig. 5, this results in reduced skin friction. However, the combustion-induced temperature rise leads to further reductions in boundary-layer densities, and therefore causes further reductions in skin friction. This is evident in comparing the skin-friction coefficients in Figs. 4 and 5 with a given surface hydrogen mass fraction. In spite of the somewhat greater hydrogen mass flows shown by Fig. 5 to be associated with a given surface hydrogen mass fraction, the skin-friction coefficients of Fig. 4 are lower than those of Fig. 5.

In both Figs. 4 and 5, the lines displaying the variation of the skin-friction coefficient with Reynolds number are parallel, showing that the ratio of the skin-friction coefficient at a given value of surface hydrogen mass fraction to the skin-friction coefficient with no hydrogen injection is independent of Reynolds number. Because the no-injection skin-friction coefficient falls with increasing Reynolds number, it follows that the skin-friction coefficient at a given surface hydrogen mass fraction also falls. However, if the hydrogen mass flow remains constant, the surface hydrogen mass fraction is reduced

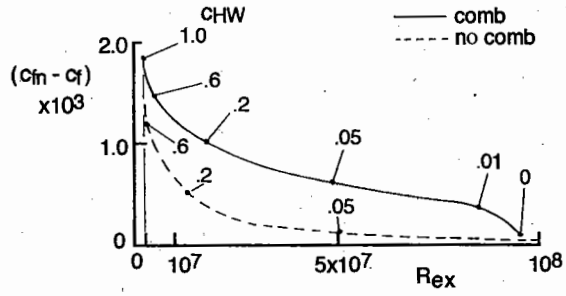

a) Skin friction

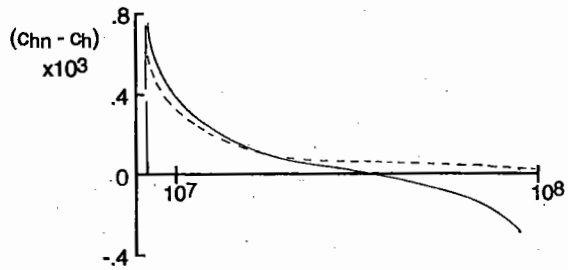

b) Heat transfer

Fig. 6 Influence of combustion: $H_e = 7.54$ MJ/kg, $T_e = 1500$ K, $T_w = 300$ K, $U_e = 3.38$ km/s, $u_j = 1.55$ km/s, and $\dot{m} = 0.20$ kg/s/m.

as the Reynolds number increases, and Figs. 4 and 5 can be used to show that the skin-friction coefficient increases with Reynolds number, as it approaches the no-injection value. When $c_{HW} = 0$, corresponding to region (iv) in Fig. 2a, the skin-friction coefficient is close to its no-injection value, indicating that the skin-friction reduction then is negligible.

Skin-Friction and Heat-Transfer Distributions

A typical downstream distribution of the reduction in skin-friction coefficient, with respect to the no-injection value c_{fn}, is shown in Fig. 6a for a constant hydrogen mass flow. Curves are presented

for hydrogen mixing with combustion and for hydrogen mixing without combustion. The associated reduction in Stanton number is shown in Fig. 6b. The skin-friction coefficient values are obtained from Figs. 4 and 5 at a hydrogen mass flow of 0.20 kg/s/m (i.e., by following the line AB in the figures). The Stanton numbers are obtained from the values of the skin-friction coefficient by applying Eq. (36), with $P_m = 1$, and Eqs. (37) and (43). The downstream decay of the surface hydrogen mass fraction is made evident by the values noted on the curves.

Surface hydrogen mass fractions approach unity at the lower values of Reynolds number, and, although the maximum values of the reduction in skin-friction coefficient occur in this region, the reduction caused by combustion with mixing is only some 50% greater than that caused by mixing alone. In passing downstream to lower values of the surface hydrogen mass fraction, the skin-friction coefficient reduction falls for combustion with mixing, but the reduction for mixing alone falls more rapidly, and combustion contributes a dominant part of the overall reduction in skin-friction coefficient. Integrating the two curves of Fig. 6a, it is found that the overall skin-friction reduction with combustion and mixing is three times the skin-friction reduction with mixing alone, and, integrating the no-injection skin-friction coefficient over the same range of Reynolds numbers, that the overall reduction is 36% of the no-injection skin-friction drag. It can be remarked that, although the major part of these effects appear to involve surprisingly low values of the surface hydrogen mass fraction, these low values correspond to substantial mole fractions.

Figure 6b shows that reductions in heat transfer, relative to the no-injection case, are approximately the same for the combustion and mixing and the mixing-alone cases. This similarity persists down to relatively low values of the surface hydrogen mass fraction and comes about because, at this stagnation enthalpy, the tendency for the lower skin friction to yield a lower heat-transfer rate in the combustion and mixing case is approximately balanced by the additional combustion related heat transfer then taking place. At the lower values of the surface hydrogen mass fraction, the heat transfer in the mixing-alone case approaches the no-injection level, but in the combustion and mixing case a reversal takes place, yielding an increase in heat transfer relative to the no-injection case. However, integrating over the range of Reynolds numbers for which the curve is drawn, it is found that, in the combustion and mixing case, there is an overall reduction of 13% with respect to the total no-injection heat transfer. The increase in local heat transfer occurs in the downstream part of the flow, where the no-injection heat transfer is a minimum.

Flow Variables

The influence of hydrogen injection velocity, surface temperature and mainstream static enthalpy on the skin-friction reduction effect is shown in Figs. 7a–7c, respectively. Figure 7a shows that, except at low velocities, the ratio of hydrogen injection velocity to mainstream velocity has very little effect on skin-friction levels.

Figure 7b shows that, at values of surface hydrogen mass fraction near unity, the proportional reduction in skin-friction coefficient is less for lower values of the surface temperature. This effect tends to be offset by the increase in no-injection skin friction, which is shown by the broken line, and this leads to a skin-friction coefficient reduction, which is independent of surface temperature. At lower values of the surface hydrogen mass fraction, the proportional reduction in skin-friction coefficient does not vary with temperature, implying that the reduction in skin-friction coefficient, and therefore the reduction in surface shear stress, increases somewhat as the surface temperature is reduced.

The static enthalpy h_e appears as the horizontal scale of Fig. 7c, and is related to the temperature scale at the top of the figure through the constant pressure specific heat, taken as $[1000 + 0.19(T - 300)]$ (J/kg)K (Ref. 21). Noting that the stagnation enthalpy is constant, the range of mainstream Mach numbers encompassed by the figure is also indicated by the scale at the bottom of the figure. It is clear that the proportional reduction in skin-friction coefficient varies very little with static enthalpy, but,

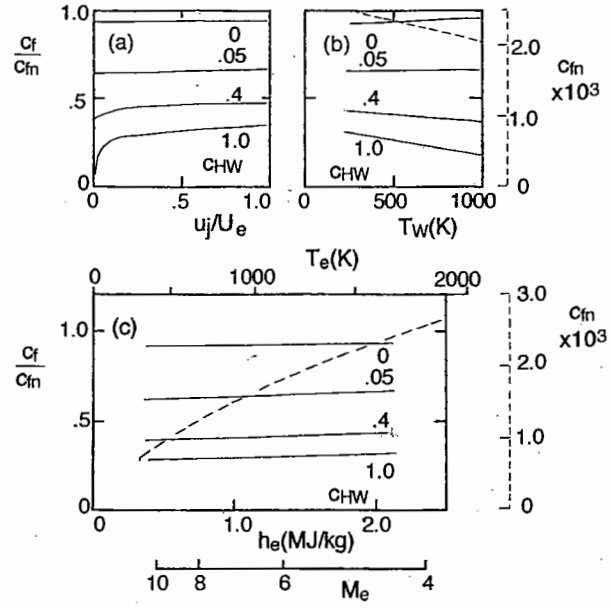

Fig. 7 Sensitivity of skin-friction reduction to hydrogen injection velocity, mainstream temperature, and surface temperature: $H_e = 7.54$ MJ/kg, $R_{ex} = 10^7$, $T_e = 1500$ K for panels a and b, $T_w = 300$ K for panels a and c, and $u_j/U_e = 0.46$ for panels b and c.

because the no-injection skin-friction coefficient varies with static enthalpy in the manner shown by the broken line, the reduction in skin-friction coefficient is least at the lower static enthalpies. Because Eq. (31) indicates that a reduced skin-friction coefficient implies a reduced value of the momentum thickness, Eq. (30) indicates that the hydrogen mass flow is also reduced by reductions in static enthalpy.

Comparison with Numerical Simulation and Experiment

Numerical Simulation

Results of the analysis are compared with the results of a numerical simulation employing finite-rate chemistry or instantaneous reaction according to Eq. (6). The code used for the simulation has been outlined in Ref. 2 and is described in more detail in Ref. 24. Briefly, it involves a k–ε turbulence model and uses a parabolic Navier–Stokes technique with a finite volume method to solve the partial differential equations. The fluxes of heat and shear stress to the wall were evaluated using wall functions, which assumed that the logarithmic law of the wall held in the fully turbulent region close to the wall.

The skin friction obtained with the analysis is compared in Fig. 8 with that predicted by the numerical simulation for flow at constant pressure. The analytical predictions cover the range of surface hydrogen mass fractions from 1.0 to 0.02 for the combustion and mixing case in Fig. 8a. The analytic and the numerical no-injection curves are in close agreement, except at low Reynolds numbers, where the numerical simulation might be affected by the arbitrary assumptions made to start the calculation. The close agreement comes as no surprise because the analytic curve is, essentially, the well-tried Van Driest II relation. It is also no surprise that, in the combustion and mixing case, the analytic curve falls closest to the instantaneous reactions curve because such reactions are assumed for the analysis. When the numerical simulation involves finite-rate chemistry, it diverges further from the analysis near a Reynolds number of 10^7, but approaches the curves for instantaneous reaction and the analysis, at larger values of Reynolds number. This convergence is also apparent at the higher hydrogen mass flow of Fig. 8b. Note the termination of the analytic curves when the surface hydrogen mass fraction becomes unity at low Reynolds numbers. This is a consequence of restricting the analysis to region (iii) of Fig. 2b.

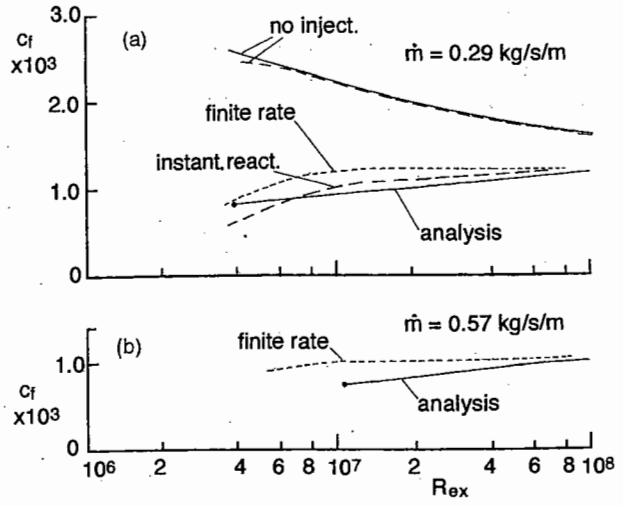

Fig. 8 Comparison of analytic and numerical results: $H_e = 7.54$ MJ/kg, $T_e = 1500$ K, $T_w = 300$ K, $U_e = 3.38$ km/s, $u_j = 1.55$ km/s for 8a, and $u_j = 1.88$ km/s for 8b.

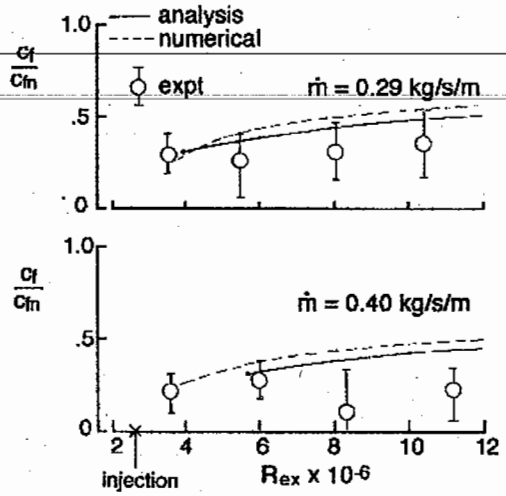

Fig. 9 Skin friction: comparison of analytic with numerical and experimental results: $H_e = 7.54$ MJ/kg, $T_e = 1500$ K, $T_w = 300$ K, $U_e = 3.38$ km/s, $u_j = 1.55$ km/s for $\dot{m} = 0.29$ kg/s/m, and $u_j = 1.77$ km/s for $\dot{m} = 0.40$ kg/s/m.

Experiment

Experimental shock-tunnel measurements of skin friction are reported in Ref. 2 and compared with numerical results. Those measurements, together with the numerical results, are compared with analytic predictions in Fig. 9 for two values of the injected hydrogen mass flow. The analytic predictions were obtained from Fig. 4 and were increased by amounts ranging up to 22% to take account of the increase in mainstream static enthalpy caused by the boundary-layer combustion-induced pressure rise along the duct in which the measurements were made. This pressure rise can be seen in Fig. 5 of Ref. 2. Assuming isentropic compression, with a constant specific heat ratio of 1.35, the distribution of mainstream static enthalpy was obtained, and Fig. 7a could then be used to yield the increase in skin-friction coefficient associated with the pressure rise. As well as exhibiting a small divergence from the numerical results, the resulting analytic predictions are seen to be reasonably consistent with the experiments in yielding a large reduction in skin friction, although at the two downstream stations the measurements tend to exhibit a somewhat larger skin-friction reduction than predicted by the analysis. This might be caused by the adverse pressure gradients in the experimental duct[2] acting on the reduced wall skin friction.

The experiments of Ref. 2 also included measurements of surface heat transfer, and the resulting Stanton numbers are compared with

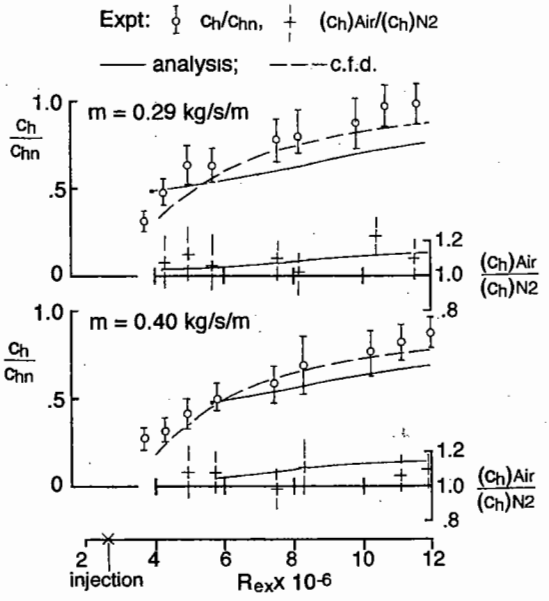

Fig. 10 Heat transfer: analysis compared with experimental results and numerical predictions: $H_e = 7.54$ MJ/kg, $T_e = 1500$ K, $T_w = 300$ K, $U_e = 3.38$ km/s, $u_j = 1.55$ km/s for $\dot{m} = 0.29$ kg/s/m, and $u_j = 1.77$ km/s for $\dot{m} = 0.40$ kg/s/m.

analytic predictions in Fig. 10. As witnessed by the ratio of Stanton number to the no-injection Stanton number, the analytic predictions deviate from the measurements and the numerical simulation by approximately the same margin as the predictions of skin-friction coefficient in Fig. 8. The heat transfer is reduced by hydrogen injection at the lower Reynolds numbers on the figure and increases with Reynolds number. It is expected to rise above the no-injection levels at higher Reynolds numbers, but, unfortunately, the range of Reynolds numbers tested did not allow this to be confirmed experimentally.

It will be recalled that, in discussing Fig. 6b, the tendency for the lower skin friction to yield a lower Stanton number in the mixing and combustion case than in the mixing alone case was balanced by the additional combustion-related heat transfer in the former case, leading to approximately equal Stanton numbers in the two cases. This was tested by comparing Stanton numbers when hydrogen was injected into air and into nitrogen. Figure 10 shows the resulting measurements compared with predictions of the analysis and demonstrates that combustion and mixing, and mixing alone, do indeed exhibit approximately equal heat transfer. This equality will depend on the ratio of combustion heat release to stagnation enthalpy and will not be expected to hold under different test conditions.

Application: Flat Plate at Incidence

The analysis has been used to explore the effect of the mass flow of injected hydrogen on the overall skin-friction drag and heat transfer with a turbulent boundary layer on a two-dimensional flat plate. The mainstream flow velocities parallel to the surface of the plate were 2, 4, and 6 km/s, corresponding to stagnation enthalpies of 2.4, 8.4, and 18.4 MJ/kg, with flight Mach numbers of 6.7, 13.3, and 20, respectively, and the mainstream temperature was 400 K. This corresponds to flight incidences of the plate surface of approximately 10, 5, and 3.5 deg, respectively. The surface temperature was 700 K, and the hydrogen was injected into the boundary layer at the surface stagnation enthalpy with a velocity of 2.4 km/s. This yielded a Mach number of the hydrogen flow at injection of 1.48, which is expected to be high enough to avoid possible difficulty in establishing a smooth flow of hydrogen in the boundary layer.[2]

The part of the surface covering a Reynolds number ranging from 3×10^6 to 1×10^8 was considered, with injection at 3×10^6, and further injection taking place at another, downstream, station as required. The second injection station was used when a higher injected

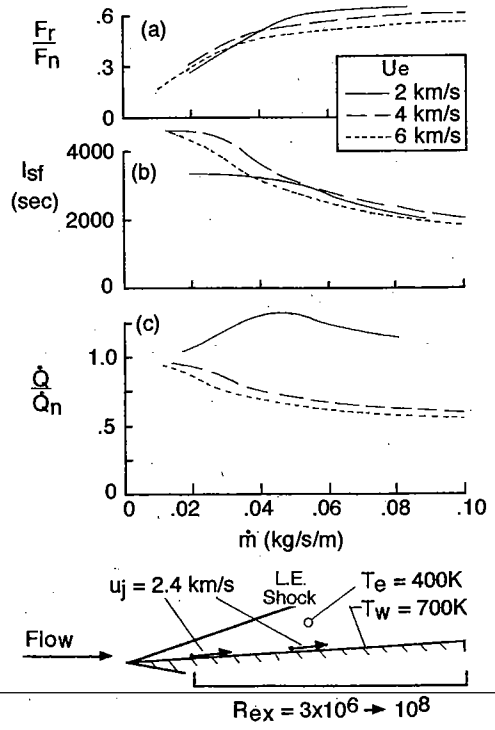

Fig. 11 Skin friction and heat transfer on a flat plate with boundary-layer combustion of hydrogen.

mass flow was desired than could be accommodated with the condition that a surface hydrogen mass fraction of unity be obtained at a Reynolds number of 3×10^6. The addition of injected mass flow would be represented on Fig. 4a by terminating the line AB at a convenient Reynolds number and beginning a new line at the same value of Reynolds number but at a higher value of injected mass flow. For the present calculations, the new line was chosen such that it began at a surface hydrogen mass fraction of unity. With the lines corresponding to the two injection stations thus defined, the distribution of skin friction along the surface could be plotted on a figure such as Fig. 6a and, by integrating along the surface, the skin-friction force could be obtained. The combined mass flow for the two injection stations would, of course, be given by the injected mass flow at the new line.

Figure 11 shows the results of these calculations. Figure 11a shows the reduction in the skin-friction force, on the plate surface, which is caused by hydrogen injection and combustion, normalized by the no-injection skin-friction force. The curves for the three velocities follow the same trend, the ratio F_r/F_n increasing with injectant mass flow and reaching values corresponding to the reduction of skin-friction drag by a factor of two or more. Further reductions of skin-friction drag, with the same injected hydrogen flow, are realized by the use of more injection stations, with calculations indicating that, at 2 km/s, increases of approximately 20% in the value of F_r/F_n could be obtained by this means. However, as it introduces additional mechanical complication into the surface this possibility was not pursued.

A reduction in the drag force can be regarded as an additional propulsive force, and the mass efficiency of the fuel in producing this force can be measured by an effective specific impulse, defined by

$$I_{sf} = (F_r + \dot{m}u_j)/(\dot{m}\bar{g}) \tag{44}$$

which is presented in Fig. 11b. The effective specific impulse has its highest value at injected mass flows, which yield the least reduction in skin-friction drag, and is reduced as the reduction in skin-friction drag increases. However, even at reduced values of approximately 2000 s, the effective specific impulse remains high enough for boundary-layer injection and combustion to be a means of combating drag, which is competitive with the direct generation of thrust.

The overall rate of heat transfer to the surface of the plate can be obtained by using the integral of the skin friction, together with Eqs. (35) and (36), respectively, for hydrogen injection with combustion and for no injection. The resulting ratio $\dot{Q}/\dot{Q}_n$ is presented in Fig. 11c. At 2 km/s, when the magnitude of combustion heat release exceeds the main stream stagnation enthalpy, the heat transfer exceeds that with no injection. However, as the stagnation enthalpy is increased, the ratio $\dot{Q}/\dot{Q}_n$ is reduced, and calculations at 3 km/s, when the combustion heat release is less than the mainstream stagnation enthalpy, show that $\dot{Q}/\dot{Q}_n$ is then less than unity. This trend is continued to the two higher velocities in Fig. 11c, where injection and combustion of hydrogen reduces the heat transfer to less than 60% of the no-injection value at the highest hydrogen mass flows. Thus, at elevated mainstream velocities this method of reducing skin-friction drag has the additional benefit of lowering the total heat transfer to the surface.

Combustion in the boundary layer can produce an increase in displacement thickness, with an associated pressure rise in the mainstream. This effect was evident in the duct experiments of Ref. 2. However, the effect can be readily modified by surface contouring, and it is not considered here.

The combustion model used assumes that no dissociation of water takes place. A measure of the propensity for dissociation to occur is the maximum temperature in the boundary layer, which is the temperature at the flame front. This temperature can be obtained from Eqs. (14) and (17). The experimental and numerical results at a stagnation enthalpy of 7.54 MJ/kg indicate that no significant dissociation occurs at this condition, and, as the calculated flame front temperature in that case is significantly exceeded only by the 6 km/s condition at low mass flows, it is concluded that, except at that condition, dissociation effects are not significant.

Conclusions

Shvab–Zeldovich coupling has been combined with the semi-empirical theory of Van Driest in an approximate analysis of hydrogen injection in a hypervelocity boundary layer. It was assumed that instantaneous, complete combustion of hydrogen and oxygen took place whenever the two came into contact and only the flow at boundary-layer stations where the surface hydrogen mass fraction lay between unity and zero was considered. Fortunately, this part of the flow provided the most interesting results in terms of the reduction of skin friction, the reduction of heat transfer, and associated mass efficiencies of hydrogen.

When the analysis was applied to a representative flow situation, it was found that the skin-friction drag reduction with mixing and combustion of the hydrogen was three times that with mixing alone. Some net reduction of heat transfer also took place, as the effect of reduced temperature gradients normal to the surface outweighed the increase caused by combustion heat release. The analysis predicted skin-friction reductions approximately 10% in excess of the results of a numerical computation with instantaneous reactions, with a somewhat greater discrepancy when a finite-rate reaction model was used. Similar differences of 10–15% were observed in comparing analytical and computational predictions of heat transfer. The analysis was also found to be consistent, to within similar limits of accuracy, with experimental measurements of skin friction and heat transfer.

The analysis was applied to flat-plate flow at mainstream velocities of 2, 4, and 6 km/s and predicted that boundary-layer injection and combustion of hydrogen would reduce the skin-friction drag on the plate to less than one-half of the no-injection value and that, when the mainstream stagnation enthalpy exceeded a value approximating the combustion heat release in air, the net heat transfer to the plate was also reduced. The mass efficiency of hydrogen injection was assessed by treating the reduction of drag as an effective thrust increase, leading to effective specific impulse values of approximately 2000 s when the aforementioned drag reductions were obtained.

The range of validity of the analysis will tend to be limited by consideration of finite-rate combustion kinetics, as this can be expected to delay the combustion heat release in the boundary layer.

This effect is evident in Fig. 8, where the use of a finite-rate numerical model increases the skin friction somewhat, and in recent experiments, which indicate that the thickness of the boundary-layer approaching the hydrogen injection station has a major effect on the boundary-layer combustion process. This type of problem can be expected to become more serious as static pressures are reduced below the value of 50 kPa used in the experiments referred to here, and it might be necessary to consider the use of ignition sources, or flameholders, within the boundary layer.

Clearly, it would be useful if the reaction rate limits to this analysis could be explored by numerical modeling of boundary-layer combustion, coupled with further experimental research. However, the analysis indicates that, when boundary-layer combustion of hydrogen does occur, it offers a promising means of controlling hypersonic turbulent skin friction.

Acknowledgments

The work was assisted by a grant from the Australian Research Council. The author thanks C. P. Goyne, who performed the experiments, and C. P. Brescianini and Drew Stephenson, who conducted the numerical analyses.

References

[1]Anderson, G. Y., McClinton, C. R., and Weidner, H. P., "Scramjet Performance," *Scramjet Propulsion*, Vol. 189, Progress in Aeronautics and Astronautics, AIAA, Reston, VA, 2000, pp. 369–446.

[2]Goyne, C. P., Stalker, R. J., and Paull, A., "Hypervelocity Skin-Friction Reduction by Boundary Layer Combustion of Hydrogen," *Journal of Spacecraft and Rockets*, Vol. 37, No. 6, 2000, pp. 740–746.

[3]Van Driest, E. R., "Turbulent Boundary Layer in Compressible Fluids," *Journal of the Aeronautical Sciences*, Vol. 18, No. 3, 1951, pp. 145–160.

[4]Van Driest, E. R., "The Problem of Aerodynamic Heating," *Aeronautical Engineering Review*, Vol. 15, No. 10, 1956, pp. 26–41.

[5]Spalding, D. B., and Chi, S. W., "The Drag of a Compressible Turbulent Boundary Layer on a Smooth Flat Plate with and Without Heat Transfer," *Journal of Fluid Mechanics*, Vol. 18, Pt. 1, 1964, pp. 117–143.

[6]Eckert, E. R. G., "Engineering Relations for Friction and Heat Transfer to Surfaces in High Velocity Flow," *Journal of the Aeronautical Sciences*, Vol. 22, No. 8, 1955, pp. 585–587.

[7]Stollery, J. L., "Supersonic Turbulent Boundary Layers: Some Comparisons Between Experiment and a Simple Theory," *Aeronautical Quarterly*, Vol. 27, May 1976, pp. 87–98.

[8]Kulgein, N. G., "Transport Processes in a Combustible Turbulent Boundary Layer," *Journal of Fluid Mechanics*, Vol. 12, 1962, pp. 417–437.

[9]Wooldridge, C. E., and Muzzy, R. J., "Measurements in a Turbulent Boundary Layer with Porous Wall Injection and Combustion," *Proceedings of the Tenth International Symposium on Combustion*, Combustion Inst., Pittsburgh, PA, 1965, pp. 1351–1362.

[10]Jones, J. W., Isaacson, L. K., and Vrecke, S., "A Turbulent Boundary Layer with Mass Addition, Combustion, and Pressure Gradients," *AIAA Journal*, Vol. 9, No. 9, 1971, pp. 1762–1768.

[11]Levin, V. A., and Larin, O. B., "Skin Friction Reduction by Energy Addition into a Turbulent Boundary Layer," AIAA Paper 2003-0036, Jan. 2003.

[12]Hefner, J. N., and Bushnell, D. M., "Viscous Drag Reduction via Surface Mass Injection," *Viscous Drag Reduction in Boundary Layers*, Vol. 123, Progress in Aeronautics and Astronautics, AIAA, Reston, VA, 1990, pp. 457–474.

[13]Hopkins, E. J., and Inouye, M., "An Evaluation of Theories for Predicting Turbulent Skin Friction and Heat Transfer on Flat Plates at Supersonic and Hypersonic Mach Numbers," *AIAA Journal*, Vol. 9, No. 6, 1971, pp. 993–1003.

[14]Hopkins, E. J., Keener, E. R., Polek, T. E., and Dwyer, H. A., "Hypersonic Turbulent Skin-Friction and Boundary Layer Profiles on Nonadiabatic Flat Plates," *AIAA Journal*, Vol. 10, No. 1, 1972, pp. 40–48.

[15]Holden, M. S., "An Experimental Investigation of Turbulent Boundary Layers at High Mach Number and Reynolds Numbers," NASA CR-112147, Nov. 1972.

[16]Goyne, C. P., Stalker, R. J., and Paull, A., "Skin Friction Measurements in High Enthalpy Hypersonic Boundary Layers," *Journal of Fluid Mechanics*, Vol. 485, 2003, pp. 1–32.

[17]Zoby, E. V., and Rumsey, C. B., "Analysis of Free-Flight Laminar, Transitional, and Turbulent Heat-Transfer Results at Free-Stream Mach Numbers Near 20 (Reentry F)," NASA TMX-2335, Sept. 1971.

[18]Anderson, J. D., Jr., *Hypersonic and High Temperature Gas Dynamics*, McGraw–Hill, New York, 1989, p. 260.

[19]Dorrance, W. H., *Viscous Hypersonic Flow*, McGraw–Hill, New York, 1962, p. 182.

[20]Zeldovich, Y. B., "On the Theory of Combustion of Initially Unmixed Gases," NACA TM 1296, June 1951.

[21]White, F. M., *Viscous Fluid Flow*, 2nd ed., McGraw–Hill, New York, 1991, pp. 28–32.

[22]Blake, L. H., "Approximate Transport Calculations for High-Temperature Air," *AIAA Journal*, Vol. 8, No. 9, 1970, pp. 1698–1701.

[23]Yamane, R., Ishihara, K., Mori, A., Park, M., Okai, H., and Oshima, S., "Recovery of Distorted Turbulent Boundary Layer and Shock/Shock Interaction through Recovering Boundary Layer," *Japan Society of Mechanical Engineers International Journal, Series B*, Vol. 40, No. 4, 1997, pp. 542–549.

[24]Brescianini, C. P., "An Investigation of the Wall-Injected Scramjet," Ph.D. Dissertation, Mechanical Engineering, Univ. of Queensland, Brisbane, Australia, March 1993.

R. Kimmel
Associate Editor